



Robust control of an electromagnetic active suspension system: Simulations and measurements

T.P.J. van der Sande^{a,*}, B.L.J. Gysen^b, I.J.M. Besselink^a, J.J.H. Paulides^b, E.A. Lomonova^b, H. Nijmeijer^a

^a Department of Mechanical Engineering, Eindhoven University of Technology, P.O. Box 513, Eindhoven 5600MB, The Netherlands

^b Department of Electrical Engineering, Eindhoven University of Technology, The Netherlands

ARTICLE INFO

Article history:

Available online 15 August 2012

Keywords:

Active suspension
Robust control
Quarter car test setup
Comfort improvement

ABSTRACT

This paper considers the control of a novel high bandwidth electromagnetic active suspension system for a quarter car model in both simulations and experiments. The nature of the control problem with multiple objectives that have to be optimized as well as the uncertain parameters of the plant call for an H_∞ -controller. By changing weighting filters different controllers can be designed, emphasizing either comfort or handling. Using the high bandwidth of the actuator comfort can be improved by 40% over the passive BMW whilst keeping suspension travel within the same limits. Using a different controller, handling can be improved up to 30%, limited by RMS actuator force.

© 2012 Elsevier Ltd. All rights reserved.

1. Introduction

A conventional car suspension is always a trade-off between comfort and handling. Over the last decade, top of the line manufacturers have therefore developed active suspension systems to enhance comfort when driving straight whilst improving handling while cornering. Current day examples are the ABC system [3] employed by Mercedes which contains a hydraulic actuator in series with a passive suspension. Whilst this system can provide energy to the suspension, a bandwidth of only 5 Hz is obtained and continuous pressurization is required making the energy demands very high. Another example is the Delphi magneto-rheological damper [2] which, under the influence of a magnetic field, can change its damping value within a specified range. Benefits of this system are its high bandwidth and low power requirement. Energy can, however, not be supplied to the system making this a semi-active system.

Various other solutions have been developed to provide active suspension, however they all suffer from either low bandwidth [19], high power demands or limited usability. The only suspension that is claimed to solve all of these problems is developed by Bose Corp. [1], details of this system are, however, not provided.

Given these drawbacks, a novel tubular permanent magnet electromagnetic actuator [9] was designed as shown in Fig. 1. It is capable of delivering direct drive in a small volume. Furthermore, the bandwidth it can achieve is much higher than that of other fully active systems. Power consumption is lower than that of a hydraulic system since no continuous pressurization is neces-

sary and energy can even be recuperated depending on the damping value and controller settings [10].

To prove the increased efficiency and bandwidth of this electromagnetic suspension a controller has to be developed. Numerous publications exist on the control of active suspension systems, for example Lee and Kim [17] considers lead-lag, LQ and fuzzy control for a brushless tubular permanent magnet actuator. Due to the limited peak force (29.6 N) of the actuator, a scaled down (sprung mass 2.3 kg, unsprung mass 2.27 kg) test setup is considered making the setup not representing a typical vehicle (sprung-unsprung ratio 10:1). Furthermore, the parameters of the setup are considered to be fixed and fully known. Performance gains up to 77% were achieved, however, no notion was made on the deterioration of suspension travel or handling. On the other hand, Lauwerys et al. [16] does use a full size quarter car setup and also includes uncertainties in the design of the controller. However, with the actuator being hydraulic, only a reductions in the sprung resonance is considered (1.5 Hz) opposed to the region where humans are most sensitive (4–10 Hz). Furthermore, RMS power requirements of the hydraulic suspension system are 500 W per corner, making the system inefficient.

This paper considers control of the active suspension using an H_∞ -controller. This control topology was chosen such that variations in the plant that occur in practice can be accounted for. Furthermore, weighting filters can be added to emphasize comfort (vertical acceleration) or handling (tire compression), whilst keeping both actuator force and suspension travel within its limits. By making use of frequency dependent weighting both objectives can be optimized in their most sensitive frequency band.

Design of the controller was done using a quarter car model based on a BMW 530i. Furthermore, a full size quarter car test

* Corresponding author. Tel.: +31 402475730.

E-mail address: t.p.j.v.d.sande@tue.nl (T.P.J. van der Sande).

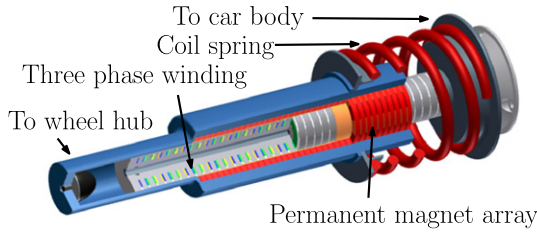


Fig. 1. Tubular permanent magnet actuator in parallel with a passive spring.

setup has been built that describes the vertical dynamics of a vehicle. Multiple suspension struts can be fitted, thereby making it possible to compare the suspension Strut of the BMW with the controlled electromagnetic suspension. It will be shown that a 41% improvement in comfort can be achieved in the frequency range of highest human sensitivity (4–10 Hz), limited by the available suspension travel. Handling can be improved by 31%, limited by the available RMS actuator force.

The outline of the paper is as follows. In Section 2 the system model will be discussed which consists of an introduction to the active suspension, the quarter car model that will be used for simulations and the road description. After this the main control problem will be presented in detail. In Section 4 the full size test setup will be shown. Design of the controller will be explained in Section 5. Results of the controllers designed can be seen in Section 6. Finally, conclusions are drawn in Section 7.

2. System model

A quarter car model will be used. For this all parameters are based on a BMW 530i. This German built saloon car is well known for its sportiness, agility and comfort. With its aluminum bonnet and front quarter panels a near to perfect 50.9/49.1% front to rear weight distribution is achieved. The front suspension system, which will be replaced by the active suspension system, is a MacPherson strut. This suspension strut has a spring stiffness of 30.01e3 N/m as is shown in Table 1, together with the other vehicle parameters. The damping of the passive suspension strut is a non-linear function of the vertical velocity and can be seen in Fig. 3. Performance of the active suspension will be compared with this passive front suspension.

Remark 1. A half or full car model is not chosen as the test setup is designed as a quarter car setup. The model is therefore also a quarter car. Furthermore, as we are most interested in comfort, which is defined by vertical acceleration of the vehicle body, a model that only describes this is chosen.

Table 1
Technical data of the BMW 530i.

Parameter	Value
Unloaded mass	1546 kg
Maximum loaded mass	2065 kg
Unsprung mass front (2 wheels)	96.6 kg
Unsprung mass rear (2 wheels)	89.8 kg
Spring stiffness	30.01e3 N/m
Tire stiffness min–max (single tire)	3.1e5–3.7e5 N/m
Weight distribution front–rear	50.9–49.1%
Maximum compression (bump)	0.06 m
Maximum extension (rebound)	0.08 m

2.1. Active suspension system

The retrofit suspension system, as shown in Fig. 1 consists of an electro-magnetic actuator in parallel with a mechanical spring to maintain the height of the vehicle. The actuator is a tubular slotted three-phase permanent magnet actuator with a maximum RMS force of 1000 N and similar suspension travel as the passive BMW suspension. Fail safe passive damping is provided by means of eddy-currents, see Fig. 3. Further specifications and its mode of operation are given in [7,8].

Three sensors are fitted on the actuator, being the sprung mass acceleration sensor, suspension travel sensor and unsprung mass acceleration sensor. The sprung acceleration sensor is fitted because it gives a direct measure of comfort of the vehicle. Second, the laser sensor is installed such that the suspension travel can be directly measured using this sensor, thereby commutation of the actuator is executed precisely. Finally, the unsprung acceleration sensor is installed to estimate the state of the tire since it is impossible to measure tire compression directly. This set of sensors provides all information necessary and is most commonly used in literature [21].

2.2. Quarter car model

A quarter car model represents one corner of a vehicle for which only the vertical dynamics are considered. Fig. 2 shows a graphical representation of the quarter car including an actuator. The body of the car is represented by the sprung mass, m_s . The wheels, brakes and part of the suspension is represented by the unsprung mass m_u . The suspension stiffness and damping are denoted by k_s and d_s respectively with the tire stiffness denoted by k_t . The degrees of freedom are the displacement of the sprung (z_s) and unsprung mass (z_u). The road displacement, z_r , is prescribed by the road profile as will be discussed below. Finally, the actuator force is denoted by F_{act} . The equations of motion are given by

$$m_s \ddot{z}_s = -k_s(z_s - z_u) - d_s(\dot{z}_s - \dot{z}_u) + F_{act} \tag{1}$$

$$m_u \ddot{z}_u = k_s(z_s - z_u) + d_s(\dot{z}_s - \dot{z}_u) - k_t(z_u - z_r) - F_{act}, \tag{2}$$

where it is assumed that tire-road contact is maintained at all time, i.e. $k_t(z_u - z_r) > 0$.

Variations that occur in the quarter car are based on physical changes such as the number of people in the car, the damper veloc-

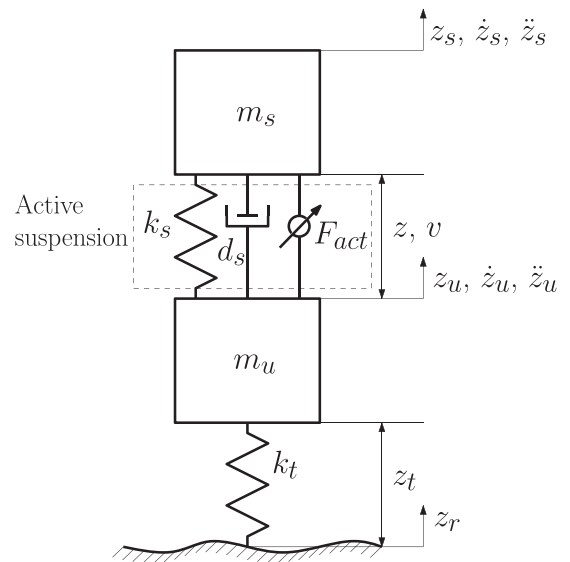


Fig. 2. Quarter car model.

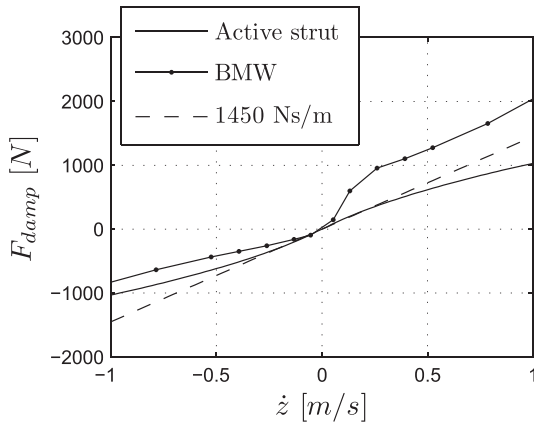


Fig. 3. Damping force of passive BMW and active suspension strut compared with linear damping.

Table 2
Parameters of the quarter car model.

Parameter	Mean value	Deviation
d_s	1450 Ns/m	$-550 + 250$ Ns/m
k_s	$30.01e3$ N/m	0 N/m
k_t	$3.4e5$ N/m	$\pm 0.3e5$ N/m
m_s	395.3 kg	$-42.77 + 75.38$ kg
m_u	48.3 kg	0 kg

ity and the load on the tire. The range of change for the sprung mass is determined by the unload and maximum mass of the vehicle, decreased with the sprung weight. The average value is based on two average weight people sitting in the car, including fuel. The second parameter that is allowed to vary is the tire stiffness as this is both a function of vertical load and inflation pressure. As Table 1 shows the tire stiffness is expected to vary between $3.1e5$ and $3.7e5$ N/m. Finally, the damping force of the electromagnetic suspension has a regressive character as a function of velocity as Fig. 3 shows. This results in a damping coefficient that is not constant. As Table 2 shows the damping value can vary between 900 and 1700 Ns/m.

2.3. Road input

A vehicle is subjected to two types of disturbances while driving: stochastic and deterministic. For the stochastic disturbances measurements [5] have shown that typical road disturbances can be represented accurately by the application of a first order filter to a white noise signal w

$$\frac{1}{vV_x} \dot{z}_r + z_r = w. \quad (3)$$

Here z_r is the vertical road input, V_x is the forward speed of the vehicle. Together with the parameter v the cut-off frequency is defined and thereby the shape of the road irregularities. Table 3 shows the parameters that have been used to create the simulated road profiles. Here, the first order low-pass output is multiplied with ψ to achieve the correct road amplitude. This gain is based on a sample time (t_s) of 0.001 s.

Table 3
Typical road parameters.

Road type	v	V_x	ψ
Smooth	0.2 rad/m	30 m/s	$0.05 \sqrt{\frac{0.001}{t_s}}$
Rough	0.8 rad/m	7.5 m/s	$0.075 \sqrt{\frac{0.001}{t_s}}$

As deterministic disturbance a 3 cm high speed bump will be used.

3. Control problem

In a car suspension multiple objectives have to be fulfilled for a car to achieve good comfort as well as good handling whilst keeping track of constraints defined by physical limitations of the car and active suspension system.

- Comfort is defined by the vertical acceleration, \ddot{z}_s , of the sprung mass. In the ISO2631-1 [14] criterion it is furthermore defined that humans are most sensitive in the frequency band between 4 and 10 Hz.
- Dynamic tire compression, z_t , is a good measure for handling. The side force a tire can create decreases when changes in vertical compression occur due to relaxation effects. This means best handling is achieved when dynamic tire compression is minimal.
- The available space in the suspension of a car is limited, this is thus defined as a constraint of the system. In case of the BMW suspension the allowed travel from minimum to maximum is 0.14 m. To make a fair comparison with the passive suspension, the active suspension is not allowed more travel than passive suspension system in the same situation.
- Thermal constraints of the active suspension limit the RMS actuator force to 1000 N.

A control topology that allows for multi variable optimization could be Linear Quadratic control, or LQG, as used in [11,13,15,22]. With this control method an optimal controller is found if the plant is fully known. A problem, however, occurs when this is not the case. As Doyle [6] has shown, there are no guaranteed stability margins for this control topology. As the plant is not fully known due to unknown variables such as the sprung mass, damping and tire stiffness, this control topology is not suitable. A method that gives the possibility of taking into account the unknown parameters whilst also allowing optimization for multiple control variables is H_∞ -control. This topology will be used in this paper.

4. Test setup

The test setup consists of a full-size quarter car model. The sprung mass (e), and unsprung mass (c) are represented by blocks of steel guided by linear bearings as Fig. 4 shows. These two masses are connected by a suspension strut (d) which in this case is either the BMW front suspension strut or the electromagnetic actuator. The tire stiffness is represented by a coil spring (b) with a constant stiffness of $352.3e3$ N/m. Road excitations are performed by a tubular industrial actuator in parallel with a spring (a) that is used to support the weight of the test setup. Control of this actuator is done by a PID controller with notches and a feed forward term counteracting disturbance forces of the active suspension system.

To assess the performance of the active suspension various sensors are installed on the test setup. Next to the sprung (\ddot{z}_s) and unsprung acceleration (\ddot{z}_u) and suspension travel (z) sensors installed on the actuator an incremental encoder is installed on the industrial actuator. This sensors is used to measure the road displacement z_r and provide feedback for the PID controller. Furthermore, a second laser sensor is installed that is used to measure the position of the unsprung mass (z_u). Together with the incremental encoder the tire compression z_t can be calculated. To determine the power, three phase-to-phase voltages as well as three phase currents are measured. The supply power is then calculated as

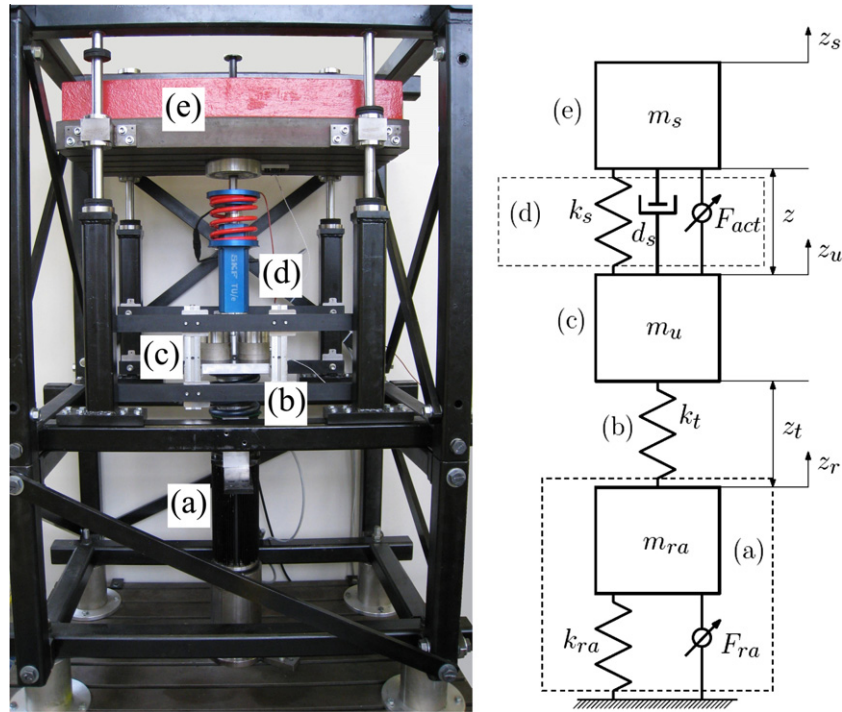


Fig. 4. Quarter car test setup, with: (a) road shaker, (b) tire spring, (c) unsprung mass, (d) suspension strut and (e) sprung mass.

$$P_s = I_a V_{ac} + I_b V_{bc}. \quad (4)$$

Experimental verification of the test setup was performed using the road signal as input. As Fig. 5 shows, measurements and simulations show good coherence up to 30 Hz. Deviations are caused by friction of the linear bearings in the test setup. Since humans are most sensitive between 4 and 10 Hz this is not a problem.

5. Controller design

For design of the H_∞ -controller, the structure as shown in Fig. 6 is used. In the perturbed plant all variations as discussed before are included as parametric uncertainties. Sensor noise is assumed to be frequency independent and is therefore modeled as white noise multiplied by a gain (W_{n1} , W_{n2} and W_{n3}) such that the amplitude of the noise matches that of the sensor noise measured on the test setup. The levels are shown in Table 4.

The disturbance input to the plant is the road disturbance and the controlled input is the actuator force calculated by the controller. All this is then put into the standard form as shown in Fig. 7 which is used for robustness and performance analysis. In this figure y_d are the inputs to the uncertainty matrix and u_Δ are the inputs to the plant resulting from the uncertainties. As disturbance input $w = z_r$ is used. The controlled output is defined as

$$y_c = [W_{z_t} z_t \quad W_{z_s} \ddot{z}_s \quad W_z (z_s - z_u) \quad W_{F_{act}} F_{act}]^T, \quad (5)$$

where each control objective as defined in Section 3 is multiplied by a weighting filter. These weighting filters will be explained in Sub-Section 5.1. Input to the controller are the measured sprung acceleration, suspension travel and unsprung acceleration,

$$v = [\dot{z}_s \quad \ddot{z}_u \quad z_s - z_u]^T. \quad (6)$$

The output of the controller is the actuator force $u = F_{act}$. Furthermore, N is the generalized plant P connected to the controller K via a lower fractional transformation

$$N = F_l(P, K) \equiv P_{11} + P_{12}K(I - P_{22}K)^{-1}P_{21}. \quad (7)$$

In total N has seven outputs. Three that couple it to the uncertainty matrix and four controlled outputs as defined by (5), these are also the external outputs of N . Four inputs are defined for N with one stemming from the road disturbance and three from the uncertainty matrix Δ .

The transfer matrix Δ is formed by pulling out the uncertainties from the plant and putting them into the uncertainty matrix

$$\Delta = \begin{bmatrix} \Delta_1 & 0 & 0 \\ 0 & \Delta_2 & 0 \\ 0 & 0 & \Delta_3 \end{bmatrix}. \quad (8)$$

Each Δ_i represents a source of uncertainty such parametric uncertainty [20]. For the greatest singular value $\bar{\sigma}$ of each Δ_i it holds that

$$\bar{\sigma}(\Delta_i) \leq 1, \forall \omega, i \in \{1, 2, 3\} \quad (9)$$

which means that each individual perturbation is stable and normalized. The parametric uncertainties as present in this problem can be found by considering (1) and (2) and writing them as

$$(\hat{m}_s + W_1 \Delta_1) \ddot{z}_s = -k_s(z_s - z_u) - (\hat{d}_s + W_2 \Delta_2)(\dot{z}_s - \dot{z}_u) + F_{act} \quad (10)$$

$$m_u \ddot{z}_u = k_s(z_s - z_u) + (\hat{d}_s + W_2 \Delta_2)(\dot{z}_s - \dot{z}_u) - (\hat{k}_t + W_3 \Delta_3)(z_u - z_r) - F_{act}. \quad (11)$$

Here, each varying parameter is represented by a mean value and an uncertain part $W_i \Delta_i$, with $i \in \{1, 2, 3\}$. Each W_i is chosen such that for each Δ_i (9) is satisfied. By defining $u_{\Delta 1} = \Delta_1 y_{d1}$ and $y_{d1} = \ddot{z}_s$ and likewise for the other uncertainties it can be written that

$$\begin{bmatrix} z_1 \\ z_2 \\ z_3 \end{bmatrix} = \begin{bmatrix} -\frac{k_s}{m_s} & -\frac{d_s}{m_s} & \frac{k_s}{m_s} & \frac{d_s}{m_s} \\ 0 & 1 & 0 & -1 \\ 0 & 0 & 1 & 0 \end{bmatrix} \begin{bmatrix} z_s \\ \dot{z}_s \\ z_u \\ \dot{z}_u \end{bmatrix} + \begin{bmatrix} \frac{1}{m_s} & 0 \\ 0 & 0 \\ 0 & -1 \end{bmatrix} \begin{bmatrix} F_{act} \\ z_r \end{bmatrix} \\ + \begin{bmatrix} -\frac{W_1}{m_s} & -\frac{W_2}{m_s} & 0 \\ 0 & 0 & 0 \\ 0 & 0 & 1 \end{bmatrix} \begin{bmatrix} u_{\Delta 1} \\ u_{\Delta 2} \\ u_{\Delta 3} \end{bmatrix}, \quad (12)$$

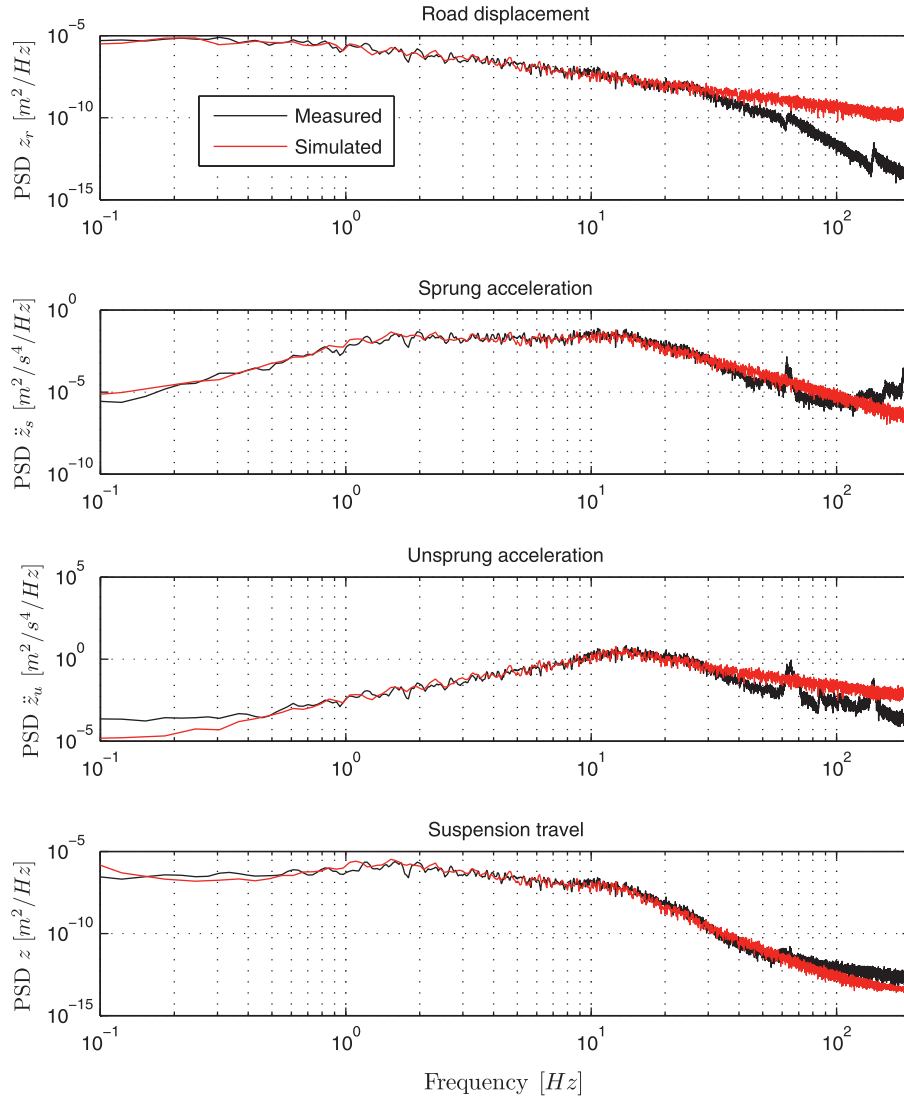


Fig. 5. Power spectral density of road signal, sprung acceleration, unsprung acceleration and suspension travel, measurement and simulation compared.

and

$$\begin{bmatrix} \dot{z}_s \\ \ddot{z}_s \\ \dot{z}_u \\ \ddot{z}_u \end{bmatrix} = \begin{bmatrix} 0 & 1 & 0 & 0 \\ -\frac{k_s}{m_s} & -\frac{d_s}{m_s} & \frac{k_s}{m_s} & \frac{d_s}{m_s} \\ 0 & 0 & 0 & 1 \\ \frac{k_s}{m_u} & \frac{d_s}{m_u} & -\frac{k_s+k_t}{m_u} & -\frac{d_s}{m_s} \end{bmatrix} \begin{bmatrix} z_s \\ \dot{z}_s \\ z_u \\ \dot{z}_u \end{bmatrix} + \begin{bmatrix} 0 & 0 \\ \frac{1}{m_s} & 0 \\ 0 & 0 \\ -\frac{1}{m_u} & -\frac{k_t}{m_u} \end{bmatrix} \begin{bmatrix} F_{act} \\ z_r \end{bmatrix} + \begin{bmatrix} 0 & 0 & 0 \\ -\frac{W_1}{m_s} & -\frac{W_2}{m_s} & 0 \\ 0 & 0 & 0 \\ 0 & \frac{W_2}{m_u} & -\frac{W_3}{m_u} \end{bmatrix} \begin{bmatrix} u_{\Delta 1} \\ u_{\Delta 2} \\ u_{\Delta 3} \end{bmatrix}. \quad (13)$$

The uncertainty matrix Δ can now be found as

$$u_{\Delta} = \begin{bmatrix} u_{\Delta 1} \\ u_{\Delta 2} \\ u_{\Delta 3} \end{bmatrix} = \begin{bmatrix} \Delta_1 & 0 & 0 \\ 0 & \Delta_2 & 0 \\ 0 & 0 & \Delta_3 \end{bmatrix} \begin{bmatrix} y_{d1} \\ y_{d2} \\ y_{d3} \end{bmatrix} = \Delta y_d. \quad (14)$$

5.1. Weighting filters

In Fig. 6 the controlled outputs are shown, these are chosen such that the control objectives as introduced in Section 3 are satisfied. Using weighting filters these objectives can be influenced in amplitude and frequency. For this, frequency dependent weighting

filters are used. Care is taken that for all weighting filters the inverse is proper by creating an equal number of poles and zeros. For the sprung acceleration a second order continuous time transfer function approximation of the ISO2631-1 standard [23] is used to emphasize human sensitivity to vertical vibrations and thereby improve comfort

$$W_{z_s} = w_{z_s} \frac{86.51s + 546.1}{s^2 + 82.17s + 1892} \frac{\frac{1}{2\pi 200}s + 1}{1}. \quad (15)$$

For the dynamic tire compression it is found that, when considering small side slip angles, variations in vertical load only influence the lateral tire force at low frequencies. A low-pass filter is therefore chosen, penalizing low frequencies

$$W_{z_t} = w_{z_t} \frac{\frac{1}{2\pi 12}s + 1}{\frac{1}{2\pi 0.6}s + 1}. \quad (16)$$

The constraint on actuator force of 1000 N RMS is fulfilled by a high-pass filter penalizing higher frequencies that are not of interest.

$$W_{Fact} = w_{Fact} \frac{\frac{1}{(2\pi 25)^2}s^2 + \frac{2.07}{2\pi 25}s + 1}{\frac{1}{(2\pi 1000)^2}s^2 + \frac{2.07}{2\pi 1000}s + 1}. \quad (17)$$

Finally, as there are no frequency requirements on the suspension travel, a gain is used to fulfill the constraint of suspension travel

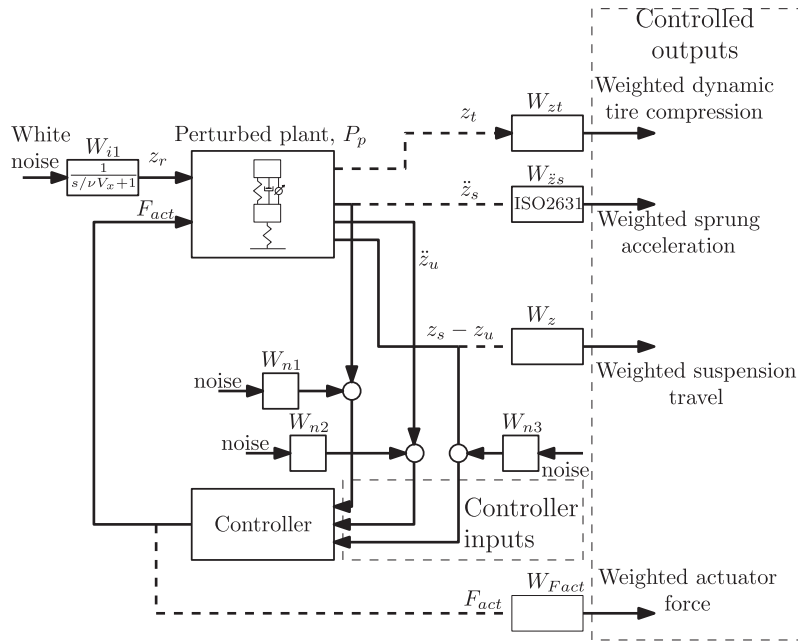


Fig. 6. Schematics used for design of robust control.

Table 4
Sensor noise.

Sensor	Deviation
Sprung acceleration sensor (W_{n1})	$\pm 0.024 \text{ m/s}^2 \text{ RMS}$
Sprung acceleration sensor (W_{n2})	$\pm 0.178 \text{ m/s}^2 \text{ RMS}$
Suspension travel sensor (W_{n3})	$\pm 0.002 \text{ m RMS}$

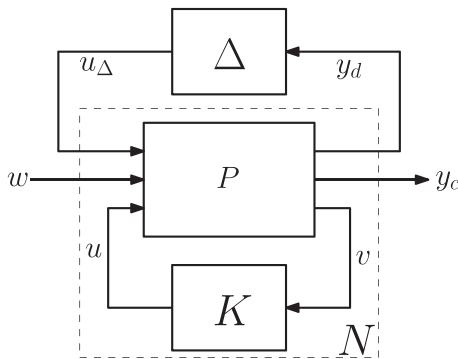


Fig. 7. Structure as used for robustness analysis.

which cannot be larger than that of the BMW suspension over a similar road

$$W_z = w_z. \tag{18}$$

The normalized form of the weighting filters is shown in Fig. 8.

By changing the amplitude of each weighting filter relative to each other either comfort or handling can be emphasized. Given the constraints two controllers were developed, one focussed on maximum comfort (limited by suspension travel) and one on best handling (limited by maximum RMS actuator force). Nine controllers, each 10% less comfortable than the previous were furthermore designed, resulting in eleven controllers in total. From this set controller 1 is designed for best comfort and controller 11 for best handling. In general it can be said that the ratio between w_{zs} and w_{zt} changes in favor of handling when this is emphasized as Fig. 9

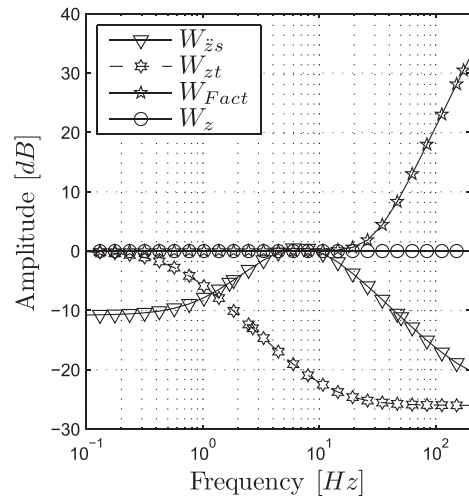


Fig. 8. Normalized weighting filters.

shows. The gain for suspension travel, w_z , remains almost constant for all eleven controllers and is only used to limit suspension travel if it surpasses the predefined limit. Finally, the multiplication factor for actuator force decreases with increasing emphasis on handling.

5.2. Robustness requirements

The main requirement of the control system is better performance, however, this better performance should not lead to possible instability. This section will discuss the methods used to assess both performance and stability.

Stability of the controlled system can be divided into two requirements; nominal stability (NS) and robust stability (RS). Nominal stability is proven by ensuring that both the generalized plant P as well as the controller K are stable. Furthermore, the poles of N are also in the left half plane, this proves nominal stability. Robust stability means that the controlled system matrix is also sta-

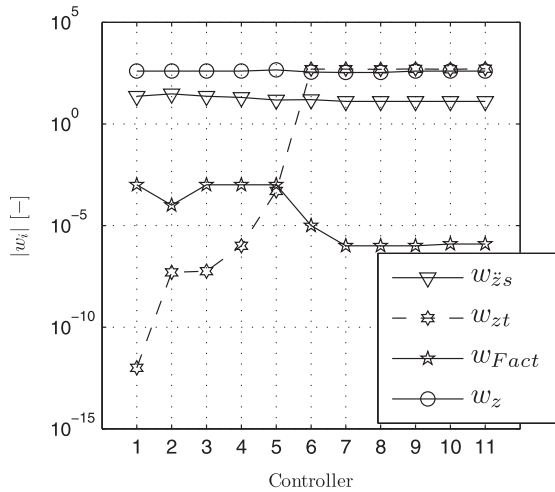


Fig. 9. Amplitude of weighting filters for all eleven controllers.

ble for all parametric perturbations. To guarantee this, the transfer function form the exogenous inputs to the outputs is defined as

$$F_u(N, \Delta) = N_{22} + N_{21} \Delta (I - N_{11} \Delta)^{-1} N_{21}. \quad (19)$$

Now assume that NS is proven, this implies that N is stable. It is furthermore assumed that Δ is stable. The only source of instability in (19) can now be $(I - N_{11} \Delta)^{-1}$, i.e. the coupling of the controlled system to the uncertainty matrix Δ . This means that when the system is nominally stable, the stability of the perturbed system is equal to the stability of the $M\Delta$ -structure, with $M = N_{11}$. Stability of the $M\Delta$ -structure is proven using the Nyquist criterion, which says that it is stable if it does not encircle the origin, this can be expressed as

$$\det(I - M\Delta) \neq 0. \quad (20)$$

The structured singular value, defined as [20]

$$\mu(M)^{-1} \equiv \min_{\Delta} \{ \bar{\sigma}(\Delta) | \det(I - M\Delta) = 0 \text{ for structured } \Delta \} \quad (21)$$

can now be used to define stability.

Now assume that both M and Δ are stable from which the requirement follows that the $M\Delta$ -structure is stable for all allowed perturbations with $\bar{\sigma}(\Delta) \leq 1, \forall \omega$ if and only if

$$\mu(M(j\omega)) < 1, \quad \forall \omega, \quad \forall \hat{\Delta}. \quad (22)$$

A value of $\mu = 1$ would mean there exists a perturbation with $\bar{\sigma}(\Delta) = 1$ that makes $I - M\Delta$ singular.

With the stability requirements satisfied, performance requirements still have to be fulfilled. This will indicate whether the controlled systems performs better than the uncontrolled system. To determine this, the worst case gain from input w to output y_c is calculated for the controlled and uncontrolled plant. Robust performance is then achieved if for all perturbations the controlled plant performs better than the uncontrolled plant. This can be formulated as

$$\frac{\mu_{\hat{\Delta}}(N_c(j\omega))}{\mu_{\hat{\Delta}}(N_u(j\omega))} < 1, \quad \forall \hat{\Delta}, \quad (23)$$

where μ is calculated with respect to the matrix

$$\hat{\Delta} = \begin{bmatrix} \Delta & 0 \\ 0 & \Delta_p \end{bmatrix}, \quad (24)$$

Δ contains the uncertainties as introduced before and Δ_p is a full complex perturbation with the same size as the number of controlled outputs. This complex perturbation is disk shaped region

in the complex plane around the nominal plant for which it holds that

$$|\Delta(j\omega)| \leq 1. \quad (25)$$

Robust performance is, however, not necessary for all outputs. Assume for instance that better comfort is required, physical limitations of the car suspension determine that a deterioration of tire compression has to happen [12]. It is therefore only required to be stable. This means that when emphasizing for comfort, tire compression will suffer and will thus not behave robustly. The opposite is also true.

5.3. Controller synthesis

As was shown, the structured singular value μ is a useful tool in analyzing the robustness of a plant and controller. As a stable system is defined by $\mu(M(j\omega)) < 1, \forall \omega$, a controller has to be designed that suffices this condition given the plant. As there is no direct method to do this, DK-iteration is performed to find a μ -optimal controller.

The idea is to find a controller that minimizes the peak value over frequency of the upper bound.

$$\mu(N) \leq \min_{D \in \mathcal{D}} \bar{\sigma}(DND^{-1}), \quad (26)$$

an attempt is made to minimize the quantity $|DN(K)D^{-1}|_{\infty}$ [18]. Here, K is an H_{∞} -controller that is synthesized while D is kept fixed, with $D \in \mathcal{D}$, a class of stable minimum-phase transfer functions. The second step is to find $D(j\omega)$ that minimizes $\bar{\sigma}(DND^{-1}(j\omega))$ with N fixed. The magnitude of $D(j\omega)$ is then fit to a stable minimum-phase transfer function $D(s)$.

Iterations continue until $|DND^{-1}|_{\infty} < 1$ or when the H_{∞} norm no longer decreases. The order of the controller resulting from this process is equal to the number of states in the plant plus the number of states in the weighting filters plus twice the number of states in $D(s)$ [4].

6. Results

As a benchmark, the characteristics of a BMW 530i are used. This means that parameters as shown in Table 1 are put into the equations introduced before. The damping as shown in Fig. 3 is furthermore used to achieve accurate results. Table 5 shows the performance of the quarter car model of the BMW on smooth and rough road. In the following section these results will be compared with the performance of the active suspension.

Measurements show that a 41% improvement in comfort can be achieved with controller 2 on the rough road, deteriorating handling by 65% as can be seen Fig. 10. This deviates 22% from the expected improvement in simulations which is primarily caused by static friction of the active suspension that was not modeled when designing the controllers. This static friction is also the cause of controller 1 not being the most comfortable controller as was expected from simulations. Furthermore, vibrations that travel through the test setup influence the measurement.

Table 5

Comparison of RMS values of simulation and measurement on quarter car test setup with BMW suspension.

	Smooth		Rough	
	Meas	Sim	Meas	Sim
\ddot{z}_s (m/s ²)	0.62	0.60	0.80	0.68
z_t (mm)	0.97	1.05	1.53	1.63
z (mm)	9.75	12.9	13.3	20.1

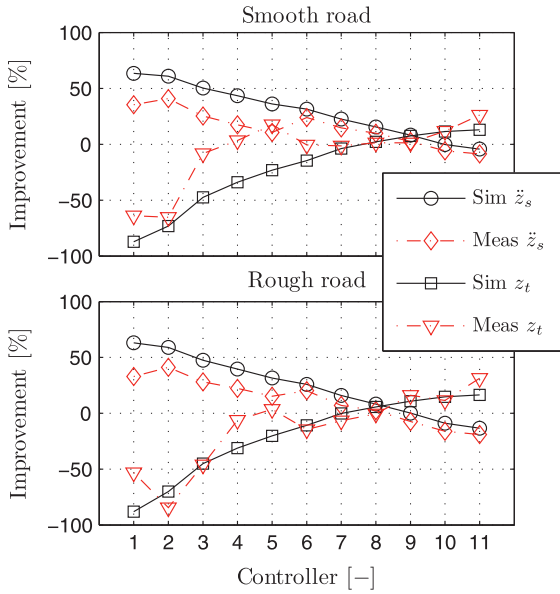


Fig. 10. Simulation and measurement results of weighted sprung acceleration and dynamic tire compression for all controllers on smooth and rough road as a percentage of passive BMW performance for the quarter car case.

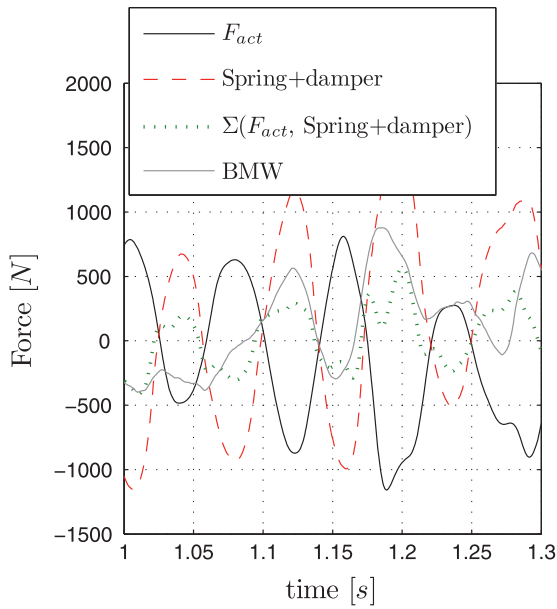


Fig. 11. Force as a function of time for both the active suspension strut and BMW suspension, with Spring + damper indication the force created by the passive spring and damper that are installed in the active strut. BMW indicates the force that the BMW suspension creates.

To make the workings of the actuator more insightful a force versus time plot is made in Fig. 11. There it can be seen that the passive force the active suspension creates is almost exactly counteracted by the active suspension thereby minimizing the force on the sprung mass and hence its acceleration.

An improvement in dynamic tire deflection of 31% can be achieved with the controller most focussed on handling (controller 11). Comfort is deteriorated by 19%. Effects of the frequency weighting filters is clearly visible here, since non-weighted vertical acceleration is deteriorated by 75% thereby showing that most vertical vibrations occur outside of the human sensitivity range. Maximum power consumption is 108 W for the best comfort controller

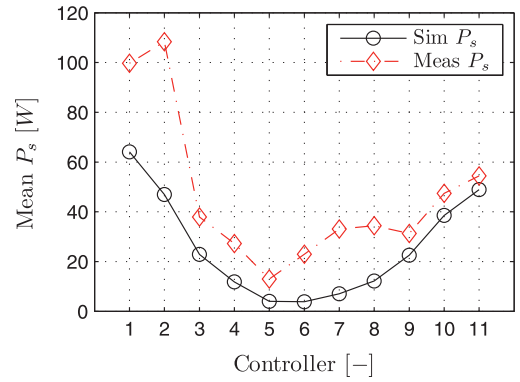


Fig. 12. Simulation and measurement results of mean supply power for all controllers on rough road.

as Fig. 12 shows. This deviation from simulations is explained by higher forces resulting from static friction and higher suspension velocities. Furthermore, switching losses are not included in simulations. This causes the measured power to be higher. The smallest power consumption is recorded for controller 5. This is caused by the performance of this controller being close to the performance of the active suspension in passive operation, thereby only requir-

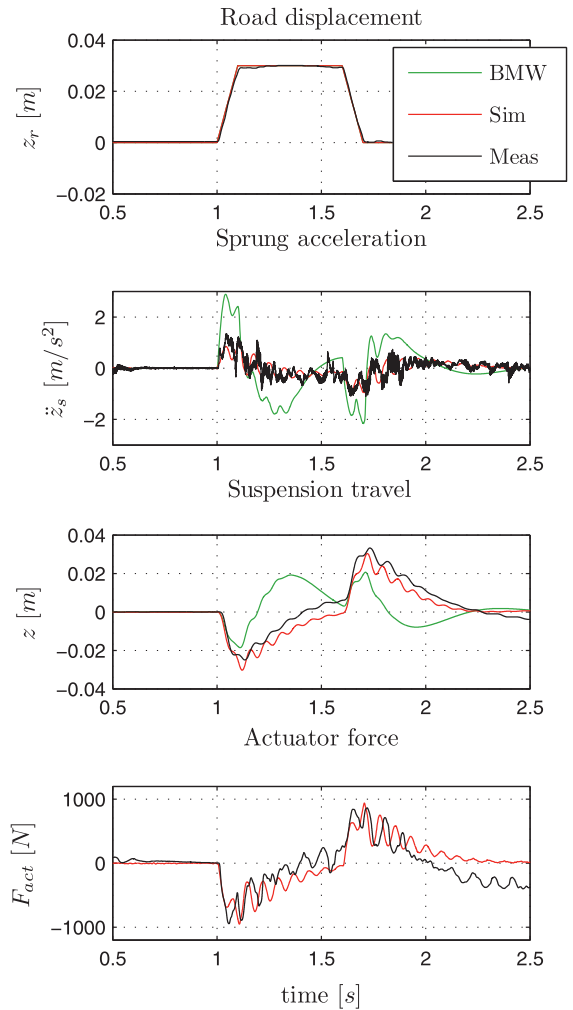


Fig. 13. Measured versus simulated road displacement, sprung acceleration, suspension travel and actuator force when driving over a speed bump with best comfort controller.

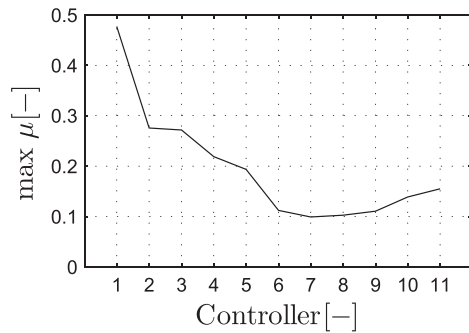


Fig. 14. Maximum structured singular value for all eleven controllers.

ing small forces. Considering the 500 W power consumption determined by Lauwerys [16], this system only consumes roughly 1/5th the power consumption of a hydraulic system whilst still offering significant improvements in both comfort and handling.

The behavior on a 3 cm speed bump has been analysed. The comfort optimal controller is loaded in an attempt to make negotiating the speed bump as comfortable as possible. As can be seen from Fig. 13 the maximum sprung acceleration is reduced with 53% compared to the BMW. This improvement, however, does cost some suspension travel. The maximum absolute actuator force is 944 N with a peak power demand of 884 W. The noise that can be observed on the sprung acceleration is caused by a setup resonance at 455 Hz, otherwise simulations and measurements match closely.

Dependency of the controller on forward velocity, as appears from (3) is little, as is already clear from the simulations performed on a deterministic road surface. Simulations with different forward speed and thus also different crossover point do not give worse results.

6.1. Stability

As was discussed in Section 5.2 robust stability is determined by the condition $\mu(M(j\omega)) < 1, \forall \omega$ if $\bar{\sigma}(\Delta) \leq 1, \forall \omega$. As Fig. 14 shows this requirement is met for all eleven controllers. All worst case gains were achieved for a damping value of 900 Ns/m, tire stiffness of 370e3 N/m and sprung mass of 352.5 kg. Note that due to the use of a grid to determine μ this is an approximation of the true μ .

Remark 2. A case study has been presented that shows the benefits of active suspension. However, the design procedure can also be used when designing for different types of active suspension systems. Furthermore, the weighting filters give a clear indication of what criteria should be used in assessing the performance of a suspension system.

7. Conclusion

A robust controller is developed for an electromagnetic suspension system using a quarter car model. Parametric uncertainties

are included in the quarter car model accounting for possible variations in the plant. Frequency dependent weighting filters are chosen such that either maximal comfort or best handling is achieved given the constraints of maximum suspension travel and actuator force. Stability of the controller is shown using the structured singular value which was smaller than 1 for all eleven controllers. Measurements show that a 41% improvement in comfort limited by suspension travel or a 31% improvement in handling determined by maximum RMS actuator force can be achieved with the active suspension compared to the passive BMW suspension. When driving over a three centimeter speed bump, comfort can be improved by 53%. Differences between measurements and simulations are explained by static friction in the active suspension. Finally, power consumption is 80% less than a hydraulic system.

References

- [1] Bose Corp. active suspension system; 2010. <<http://www.bose.com>>.
- [2] Delphi magnaride semi-active suspension; 2010. <<http://delphi.com>>.
- [3] Mercedes ABC; 2010. <http://500sec.com/abc-active-body-control>.
- [4] Damen A, Weiland S. Robust control. Lecture Notes with robust control course TUE; 2001.
- [5] Dodds C, Robson J. The description of road surface roughness. *J Sound Vib* 1973;31:175–83.
- [6] Doyle J. Guaranteed margins for LQG regulators. *IEEE Trans Autom Control* 1978;23:756–7.
- [7] Gysen B, Jansen J, Paulides J, Lomonova E. Design aspects of an active electromagnetic suspension system for automotive applications. *Ind Appl IEEE Trans* 2009;45:1589–97.
- [8] Gysen B, Paulides J, Encica L, Lomonova E. Slotted tubular permanent magnet actuator for active suspension systems. In: The 7th international symposium on linear drives for industry applications; 2009b. p. 292–95.
- [9] Gysen B, Paulides J, Janssen J, Lomonova E. Active electromagnetic suspension system for improved vehicle dynamics. *IEEE Trans Veh Technol* 2010;59:1156–63.
- [10] Gysen B, van der Sande T, Paulides J, Lomonova E. Efficiency of a regenerative direct-drive electromagnetic active suspension. In: VPPC conference; 2010b.
- [11] Gysen B, van der Sande T, Paulides J, Lomonova E. Efficiency of a regenerative direct-drive electromagnetic active suspension. *IEEE Trans Veh Technol* 2011;60:1384–93.
- [12] Hedrick J, Butsen T. Invariant properties of automotive suspensions. *Proc Inst Mech Eng* 1990;204:21–7.
- [13] Hrovat D. Survey of advanced suspension developments and related optimal control applications. *Automatica* 1997;33:1781–817.
- [14] ISO. ISO2631-1:1997:Mechanical vibration and shock – evaluation of human exposure to whole-body vibration. Technical report, international organization for standardization. Geneva – Switzerland; 1997.
- [15] de Jager A. Comparison of the two methods for the design of active suspension systems. *Optim Control Appl Methods* 1991;12:172–88.
- [16] Lauwerys C, Swevers J, Sas P. Robust linear control of an active suspension on a quarter car test-rig. *Control Eng Pract* 2005;13:577–86.
- [17] Lee S, Kim W. Active suspension control with direct-drive tubular linear brushless permanent-magnet motor. *IEEE Trans Control Syst Technol* 2010;18:859–70.
- [18] Lind R, Packard A. Evaluating d–k iteration for control design. In: Proceedings of the American control conference. p. 2792–97.
- [19] Münster M, Mair U, Gilsdorf H, Thoma A, Müller C, Hippe M, et al. Electromechanical active body control. *ATZ Worldwide* 2009:44–9.
- [20] Skogestad S, Postlethwaite I. Multivariable feedback control. Wiley; 2007.
- [21] van de Wal M, de Jager B. Actuator and sensor selection for an active vehicle suspension aimed at robust performance. *Int J Control* 1998;79:70–720.
- [22] Venhovens PJ. Optimal control of vehicle suspensions, Ph.D. thesis. Technical University Delft; 1994.
- [23] Zuo L, Nayfeh S. Low order continuous-time filters for approximation of the ISO2631-1 human vibration sensitivity weightings. *J Sound Vib* 2002;265:459–65.